Geochemistry, Geophysics, Geosystems

Supporting Information for

Evidence for Low-pressure Crustal Anatexis During the Northeast Atlantic Break-up

A.M. Morris[1], S. Lambart[1], M.A. Stearns[2], J.R. Bowman[1], M.T. Jones[3], G.T.F. Mohn[4], G. Andrews[5], J. Millet[6,7], C. Tegner[8], S. Chatterjee[9], J. Frieling[10], P. Guo[11], C. Berndt[12], S. Planke[3,7,] C.A., Alvarez Zarikian[13], P. Betlem[3,14], H. Brinkhuis[15], M. Christopoulou[16], E. Ferre[17], I.Y. Filina[18], D. Harper[1], D.W. Jolley[6], J. Longman[19], R.P. Scherer[16], N. Varela[20], W. Xu[21], S.L. Yager[22], A. Agarwal[23], V.J. Clementi[24]

[1]Geology & Geophysics Department, University of Utah, Salt Lake City, UT, USA, [2]Department of Earth Sciences, Utah Valley University, Orem, UT, USA, [3]Department of Geosciences, University of Oslo, Oslo, Norway ,[4]Laboratoire Géosciences et Environnement Cergy, University of Cergy-Pontoise, Cergy, France, [5]School of Environmental Sciences, University of Hull, Hull, UK, [6]Department of Geology and Geophysics, University of Aberdeen, King's College, Aberdeen, UK, [7]Volcanic Basin Energy Research AS, Høienhold, Oslo, Norway, [8]Department of Geoscience, Aarhus University, Aarhus, Denmark, [9]Earthquake Research Institute, The University of Tokyo, Bunkyō, Tokyo, Japan, [10]Department of Earth Sciences, The University of Oxford, Oxford, UK, [11]Institute of Oceanology, Chinese Academy of Sciences, Qingdao, China, [12]GEOMAR Helmholtz Centre for Ocean Research Kiel, Kiel, Germany, [13]International Ocean Discovery Program, Texas A&M University, College Station, TX, USA, [14]Department of Artic Geology, The University Centre in Svalbard, Svalbard, Norway, [15]NIOZ Royal Netherlands Institute for Sea Research, Den Burg, Texel, Netherlands, [16]Department of Earth, Atmosphere and Environment, Northern Illinois University, DeKalb, IL, USA, [17]School of Geoscience, University of Louisiana at Lafayette, Lafayette, LA, USA, [18]Department of Earth and Atmospheric Sciences, University of Nebraska, Lincoln, NE, USA, [19]Department of Geography and Environmental Science, Northumbria University, Newcastle Upon Tyne, UK, [20]Department of Geosciences, Virginia Tech, Blacksburg, VA, USA, [21]School of Earth Sciences and the SFI Research Centre in Applied Geosciences, University College Dublin, Dublin, Ireland, [22]Department of Environment, Geology, and Natural Resources, Ball State University, Munice, IN, USA, [23]Applied Structural Geology, Department of Earth Sciences, Indian Institute of Technology Kanpur, Kanpur, India, [24]Department of Marine and Coastal Sciences, Rutgers University, New Brunswick, NJ, USA

Contents of this file

Additional Supporting Information (Files uploaded separately)

Introduction

Data provided here includes supplemental figures as referenced in the main text and the references listed in the supplementary material. Additional supplemental tables are uploaded into a single, separate Excel file. These include all individual raw data analyses for each type of data collected for the study as well as the analytical error for any secondary standard materials.

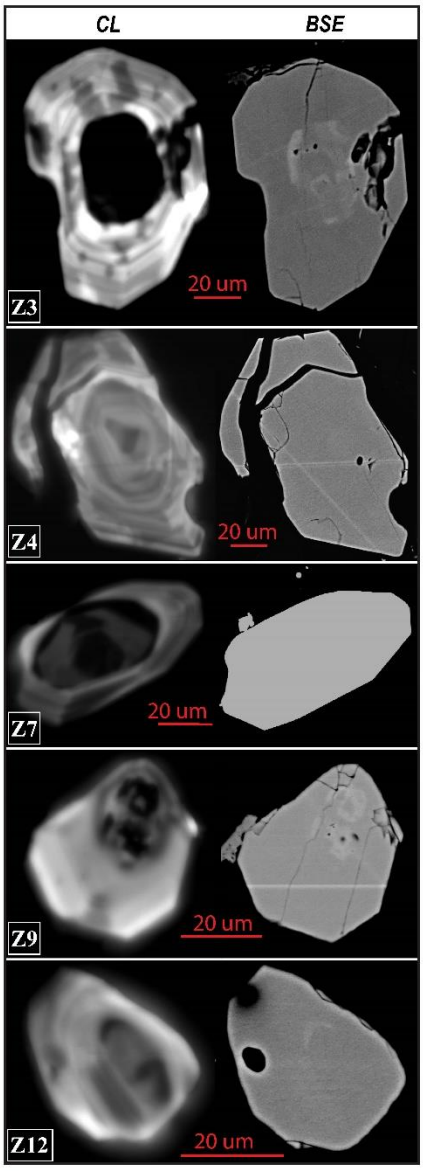

Figure S1. Cathodoluminesence (CL) and back-scattered electron (BSE) images of zircon grains presented in Fig. 10.

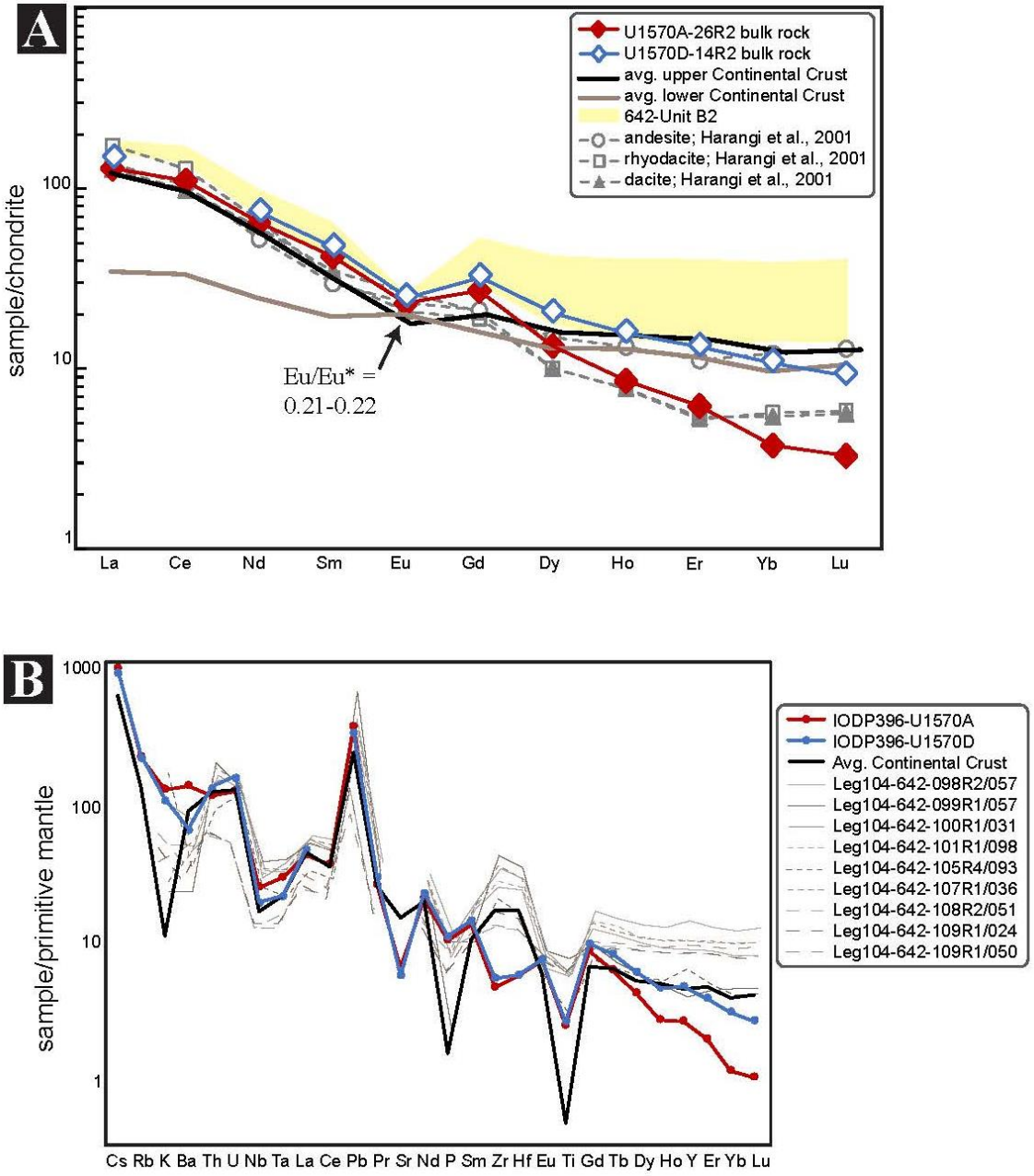

Figure S2. Chondrite-normalized (McDonough & Sun, 1995) bulk rock rare earth element (REE) concentrations for the two U1570 dacitic samples, compared with the average composition for the upper and lower continental crust (Rudnick & Gao, 2003), with the range of concentrations in Unit B2 for ODP 642E (yellow area, Meyer *et al.*, 2009a) and concentrations in calc-alkaline volcanic rocks from the Northern Pannonian Basin in Spain (gray symbols; Harangi *et al.*, 2001).

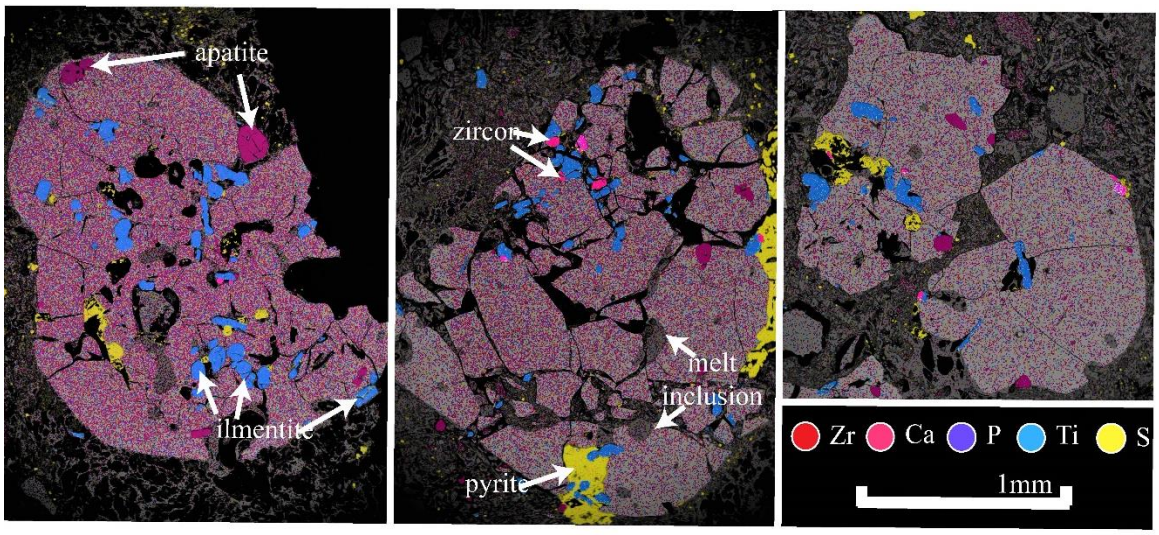

Figure S3. SEM-EDS maps of garnets from sample U1570A-26R2-4 showing the diversity of inclusions: ilmenite (blue), apatite (purple), zircon (bright pink), pyrite (yellow), and melt (dark gray). The scale bar is the same for all maps.

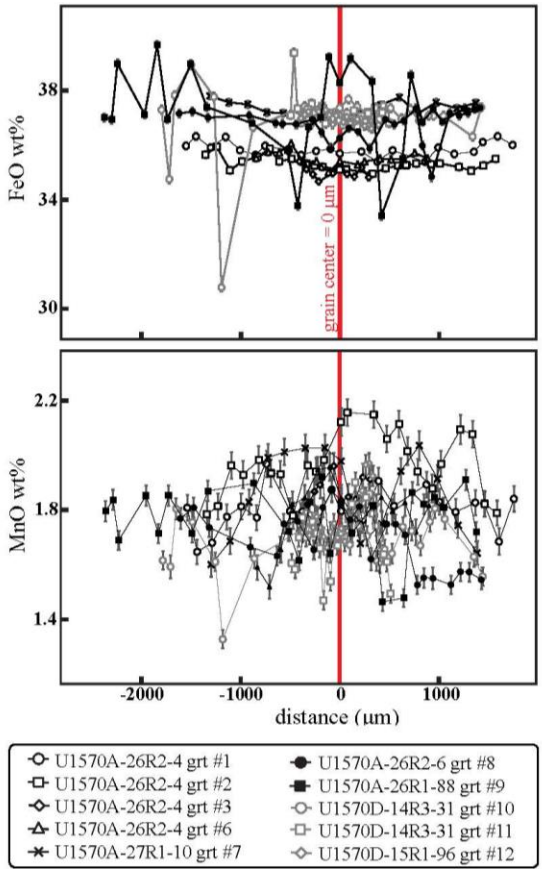

Figure S4. FeO (wt%) and MnO (wt%) profiles across garnet grains. Grain centers are represented by 0 µm red lines. Error bars represent the analytical uncertainty, 0.004 wt% and 0.03 wt%, respectively.

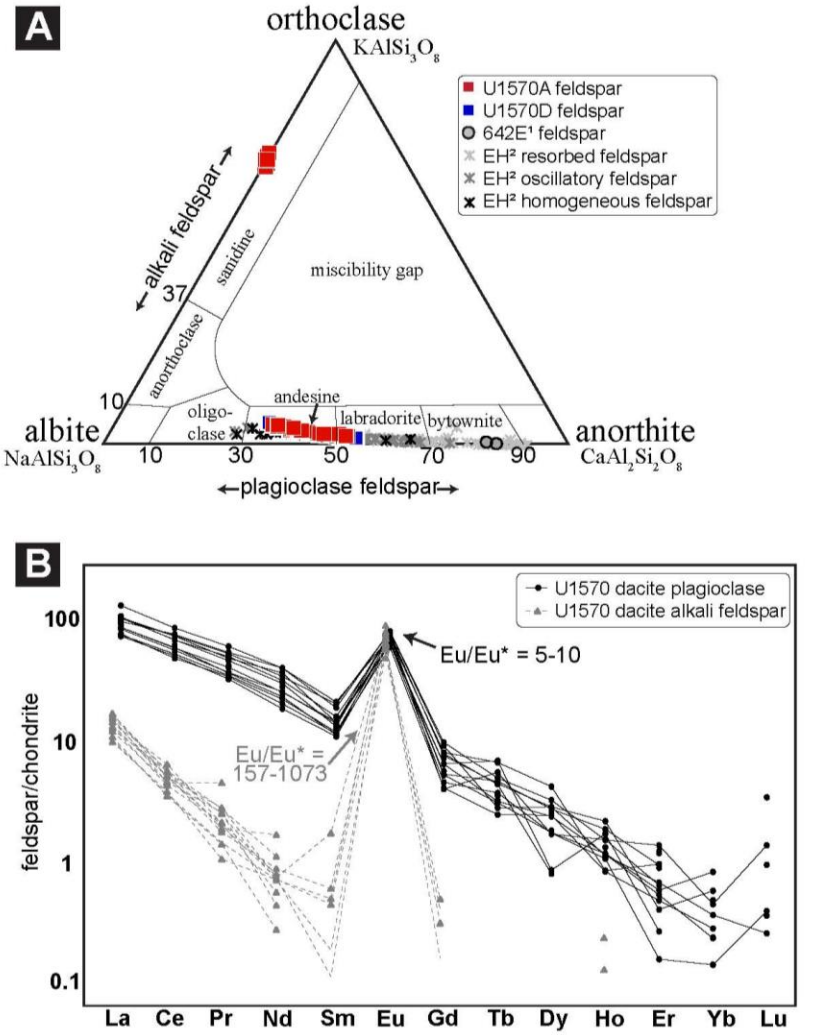

Figure S5. (A) Feldspar ternary classification diagram. Plotted are the alkali feldspar and plagioclase grains analyzed in the dacite samples from boreholes U1570A (red squares) and U1570D (blue squares) and plagioclase from 642E dacite (grey circles; Parson *et al.*, 1989). Data are compared with plagioclase from El Hoyazo (asterisks; Hiwatashi et al., 2021) separated in three groups based on their texture: Resorbed and patchy (light grey), oscillatory zoning (dark grey) and homogeneous (black). (B) Chondrite-normalized (McDonough & Sun, 1995) feldspar REE concentrations. Plotted are plagioclase (black) and alkali feldspars (gray) from our samples.

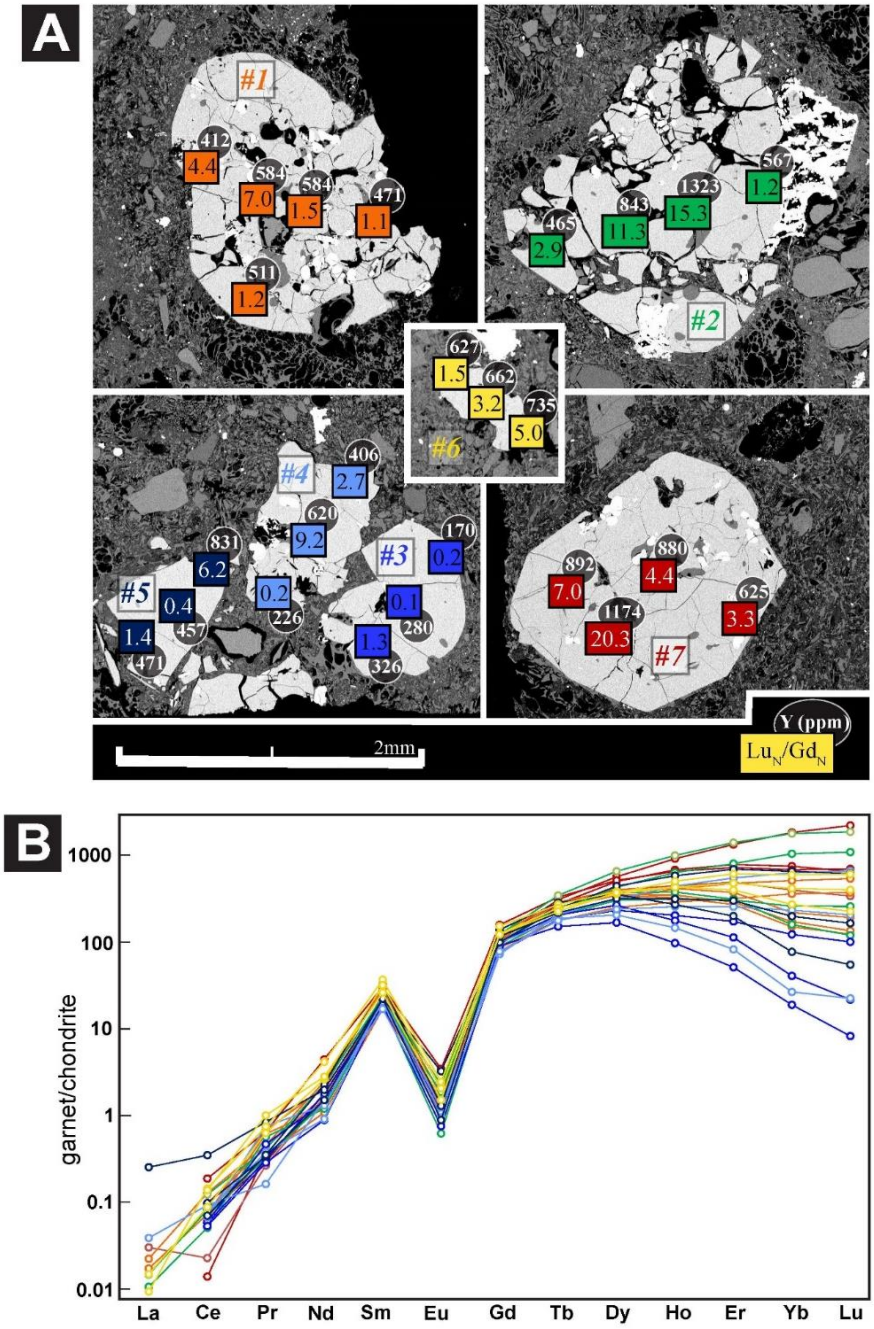

Figure S6. (A) SEM-BSE images of garnet grains analyzed by LA-ICP-MS. Garnets are numbered (from #1 to #7) according to how they are referred to in the text. Analysis locations are represented by colored squares; values on colored squares are the corresponding HREE slopes (i.e., Lu_N/Gd_N, chondrite-normalized ratio). Values in black circles are the Y (ppm) concentrations at the same location. Garnets #1, #2, #4 and #6 are all from the same sample (U1570A-26R2-4), while garnet #7 is from a sample near the base of the dacitic unit (U1570A-27R1-10). (B) Chondrite-normalized (McDonough & Sun, 1995) garnet REE concentration for each individual analysis performed on each of the seven garnets; colors correspond to those used in (A).

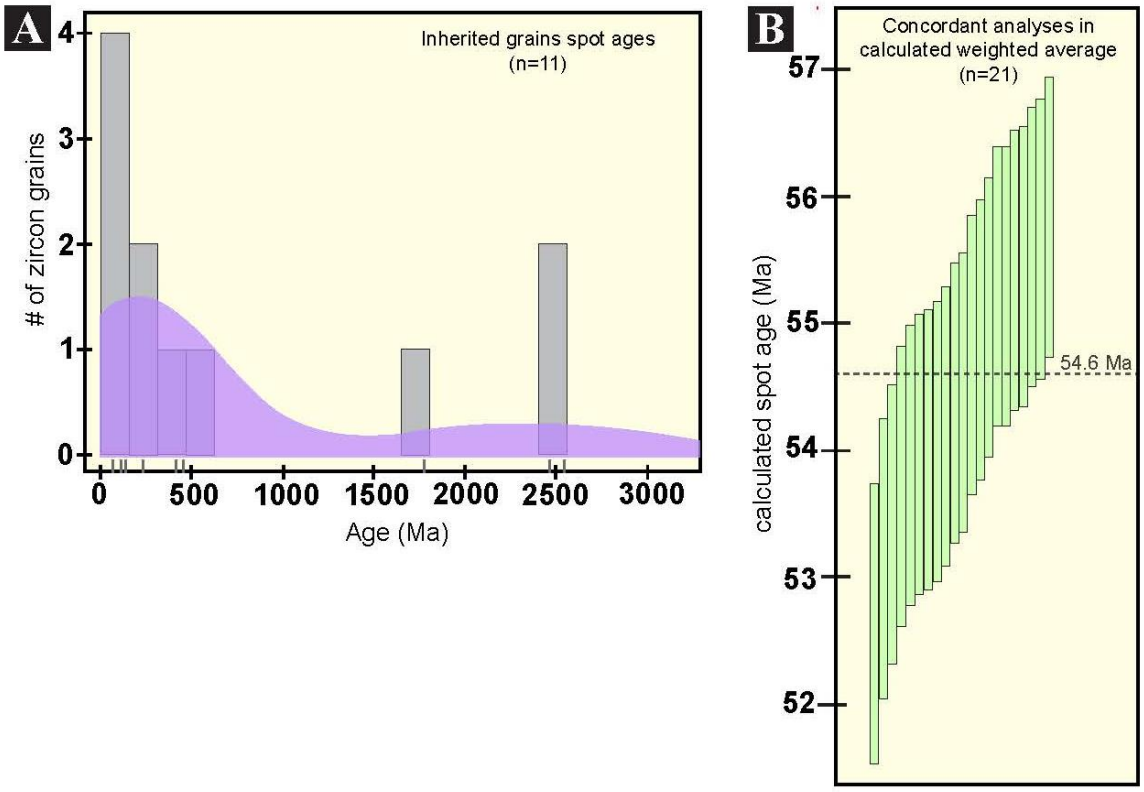

Figure S7. (A) Kernel density estimate (KDE) plot for the calculated spot ages of zircon grains in population #2 as defined by Fig. 10. (B) Calculated spot ages for young radiogenic, concordant analyses (population #1). The 54.6 Ma line represents the weighted mean for these analyses.

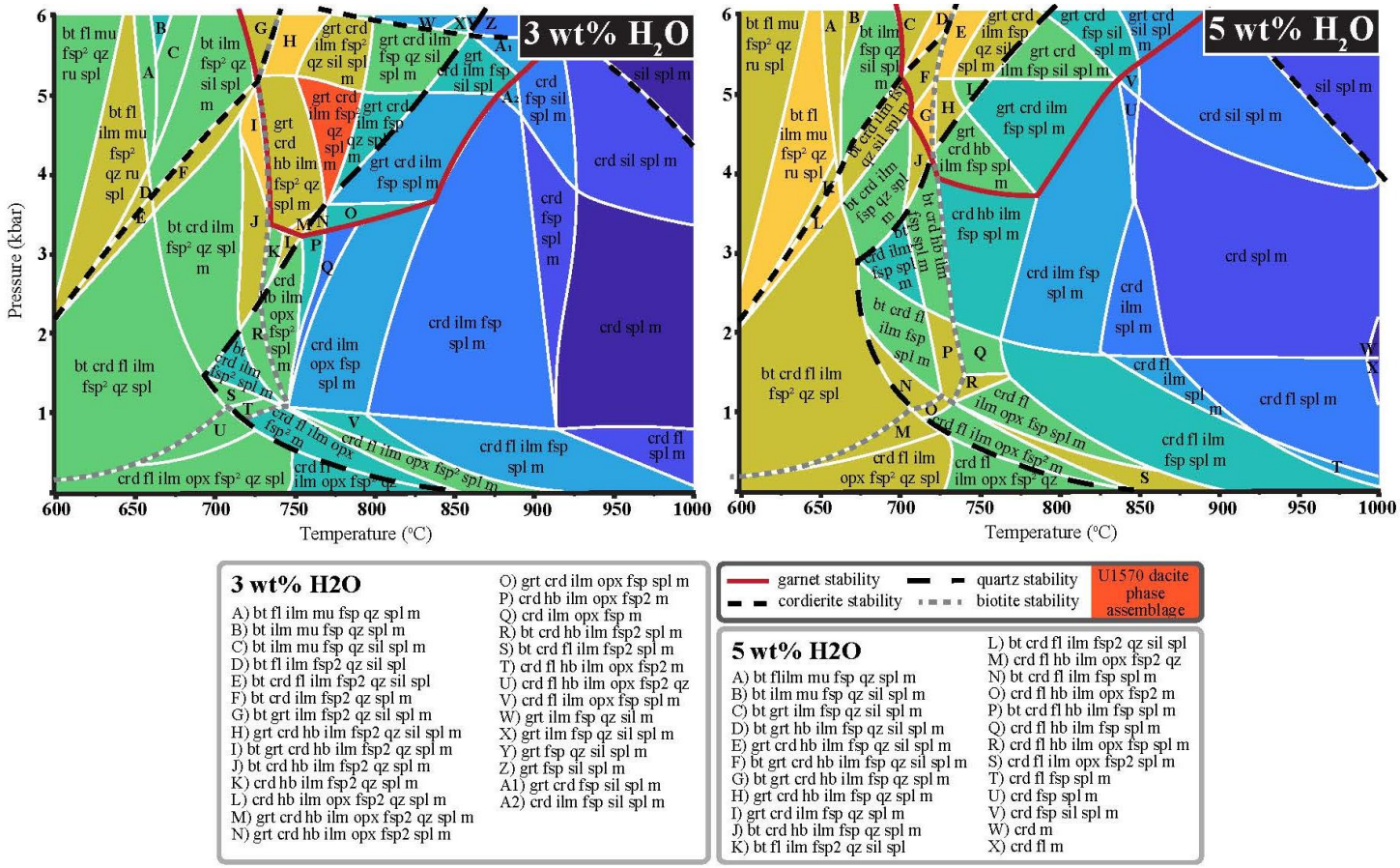

Figure S8. Pseudosections calculated with MAGEMin (Riel *et al.*, 2022) from the sample U1570-26R2-51-54 bulk rock composition of the dacite with 3wt % and 5 wt% H_2O contents. Colored fields ranging from blue to yellow represent an increasing number of phases in an assemblage; the dark orange field (H) represents the one that reproduced the observed assemblage in natural samples. Color code and abbreviations are the same as in Figure 6 in the main text.

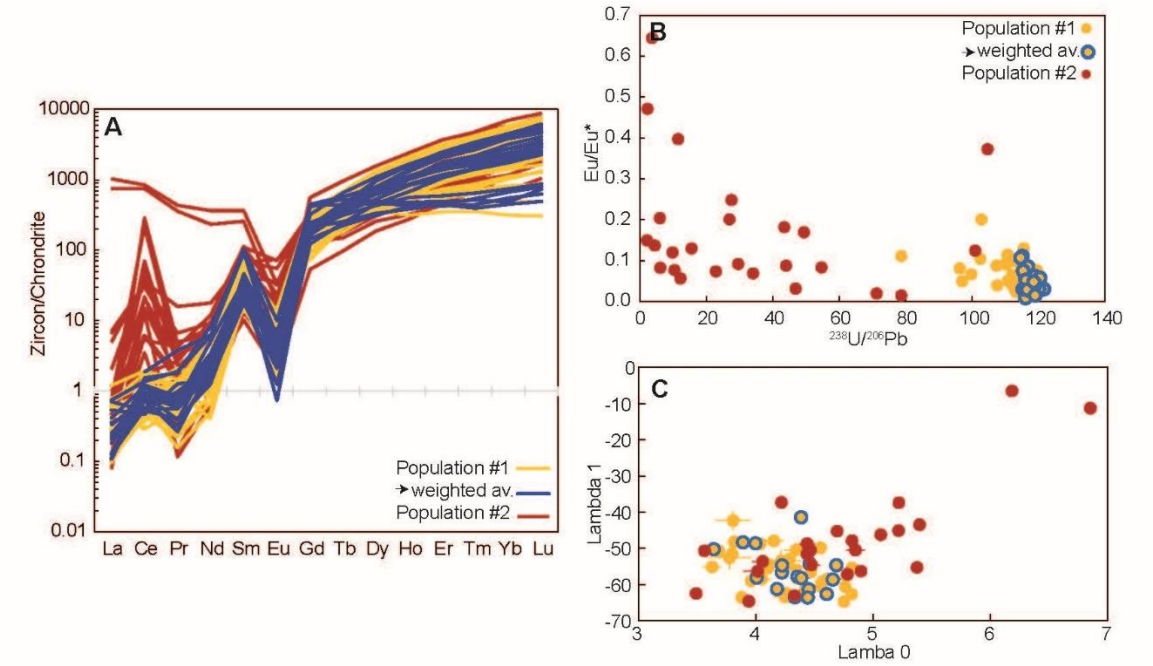

Figure S9. (A) Chondrite-normalized (McDonough & Sun, 1995) zircon REE concentration diagrams. (B) Eu anomalies (Eu/Eu*) vs. $^{238}U/^{206}Pb$ ratio for zircon analyses. (C) Shape coefficients l0 and l1 for each analyzed zircon calculated using BLambdaR online software (Anenburg and Williams, 2022). Analyses for which La is below the limit of detection are excluded. Calculations were set up excluding Ce and Eu and without including tetrads in fitting. On each panel, populations #1 (including zircons used for the weighted average) and #2 are as defined in Fig. 10.

Table S1. Composition, reproducibility and accuracy of the secondary standards during LA-ICP-MS and LASS analytical sessions.

Table S2. Dacite bulk concentrations.

Table S3. Major element oxide concentrations for individual analyses on major phases in the dacite.

Table S4. Trace element concentrations for individual analyses on major phases in the dacite.

Table S5. Carbon and nitrogen concentrations for sediments near the dacite.

Table S6. Hg concentration data for sediments near the dacite.

Table S7. Petrochronology data on zircons.

Supplementary References

Anenburg, M., & Williams, M. J. (2022). Quantifying the tetrad effect, shape components, and Ce–Eu–Gd anomalies in rare earth element patterns. *Mathematical Geosciences*, *54*(1), 47-70.

Elhlou, S., Belousova, E., Griffin, W. L., Pearson, N. J., & O'Reilly, S. Y. (2006). Trace element and isotopic composition of GJ-red zircon standard by laser ablation. *Goldschmidt Conference Abstracts*, *1*. doi:10.1016/j.gca.2006.06.1383

Jochum, K. P., Nohl, U., Herwig, K., Lammel, E., Stoll, B., & Hofmann, A. W. (2005). GeoReM: A new geochemical database for reference materials and isotopic standards. *Geostandards and Geoanalytical Research*, *29*, 333–338.

Jochum, K. P., Weis, U., Stoll, B., Kuzmin, D., Yang, Q., Raczek, I., Jacob, D. E., Stracke, A., Birbaum, K., Frick, D. A., Günther, D., & Enzweiler, J. (2011). Determination of reference values for NIST SRM 610-617 glasses following ISO guidelines. *Geostandards and Geoanalytical Research*, *35*(4), 397–429.

Lambart, S., Hamilton, S., Lang, O. I. (2022). Compositional variability of San Carlos olivine. *Chemical Geology, 605*, 120968. https://doi.org/10.1016/j.chemgeo.2022.120968

McDonough, W. F., & Sun, S. (1995). The composition of the Earth. *Chemical Geology*, *120*, 223–253.

Meyer, R., Hertogen, J., Pedersen, R. B., Viereck-Götte, L., & Abratis, M. (2009). Interaction of mantle derived melts with crust during the emplacement of the Vøring Plateau, N.E. Atlantic. *Marine Geology*, *261*(1–4), 3–16. https://doi.org/10.1016/j.margeo.2009.02.007

Parson, L., Viereck, L., Love, D., Gibson, I., Morton, A., & Hertogen, J. (1989). The petrology of the lower series volcanics, ODP Site 642. *Proceeding of the Ocean Drilling Program, Scientific Results*, *104*, 419–428.

Riel, N., Kaus, B. J. P., Green, E. C. R., & Berlie, N. (2022). MAGEMin, an Efficient Gibbs Energy Minimizer: Application to Igneous Systems. *Geochemistry, Geophysics, Geosystems*, *23*(7). doi.org/10.1029/2022GC010427

Rudnick, R. L., & Gao, S. (2003). Composition of the Continental Crust. *Treatise on Geochemistry*, *3*, 1–64.

Sláma, J., Košler, J., Condon, D. J., Crowley, J. L., Gerdes, A., Hanchar, J. M., Horstwood, M. S. A., Morris, G. A., Nasdala, L., Norberg, N., Schaltegger, U., Schoene, B., Tubrett, M. N., & Whitehouse, M. J. (2008). Plešovice zircon - A new natural reference material for U-Pb and Hf isotopic microanalysis. *Chemical Geology*, *249*(1–2), 1–35. doi.org/10.1016/j.chemgeo.2007.11.005